2001-01-1463

Effect of Viscoelastic Patch Damping on Casing Cover Dynamics

Jun Y. Kim and Rajendra Singh
The Ohio State University

ABSTRACT

Many automotive components and sub-systems require viscoelastic damping treatments to control noise and vibration characteristics. To aid the dynamic design process, new approaches are needed for modeling of partial damping treatments and characterization of the overall dynamic behavior. The analytical component of the design process is illustrated via the transmission casing cover, along with supporting experiments. First, the vibration response of production casing plates is examined, with and without the constrained layer treatment. A modified flat plate is employed along with a generic housing that provides the realistic boundary conditions for subsequent work. A simplified analytical damping model for constrained viscoelastic layer damping is suggested based on assumed modal functions. Using the analytical model, design guidelines in terms of optimal patch shapes and locations are suggested. Natural frequency shifts associated with patch damping treatments are predicted and successfully compared with measured data.

INTRODUCTION

Constrained viscoelastic layer damping treatment can effectively and economically control noise and vibration for many vehicle components. A partial damping treatment is desirable in order to reduce the additional cost and mass of the damping treatment. To maximize the benefit, the size and location of damping patches must be optimized. Changes in structural dynamic characteristics should be predicted. For this purpose, an analytical or computational model is required. The objective of this study is therefore to suggest a simplified analytical damping model that will provide insight into the effects of a constrained layer damping treatment. As a dominant effect of the damping treatment, attenuation of vibration levels is expected. Energy dissipation can also be assessed by the strain energy of the damping layer. Damping treatments also shift natural frequencies. The natural frequency shift could be related to mass and stiffness loading introduced by the damping patch. Mass loading effects can be analyzed by comparing the kinetic energy of the damping patch with that of the undamped base structure. Likewise, stiffness loading can be estimated by the relative strain energy of the damping patch with respect to the undamped structure.

EXPERIMENTAL PROCEDURE

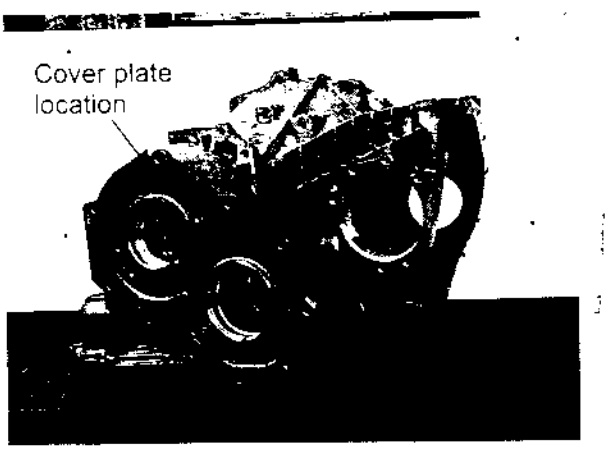

Figure 1. Original transmission casing

Figure 1 shows a transmission casing, which provides generic boundary conditions for plate structure. For the structural modal experiments, the modified casing of Figure 2 is used. Based on preliminary measurements and the results of previous work [1], the transmission casing is stiffened by attaching thick steel plates which decouples the casing from the cover plate up to 1 kHz. Figure 3 shows the schematics of experimental setup. The cover plate is fastened to the casing via 10 bolts of uniform torque. Most of the experiments are conducted at room temperature (22 ± 2 °C) and the effect of temperature on the property of damping material is ignored. The system is excited by an electromagnetic shaker through one of the bolts from the back of the casing structure. This simulates the realistic excitation since the plate is excited through its boundary. Cross point accelerance (a/F) spectra are measured at numerous points on the plate using a non-contacting method, the scanning laser vibrometer. Here, a is the acceleration and F is the dynamic force.

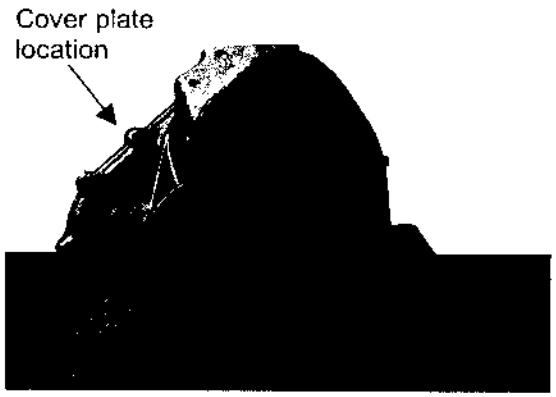

Figure 2. Modified stiffened casing

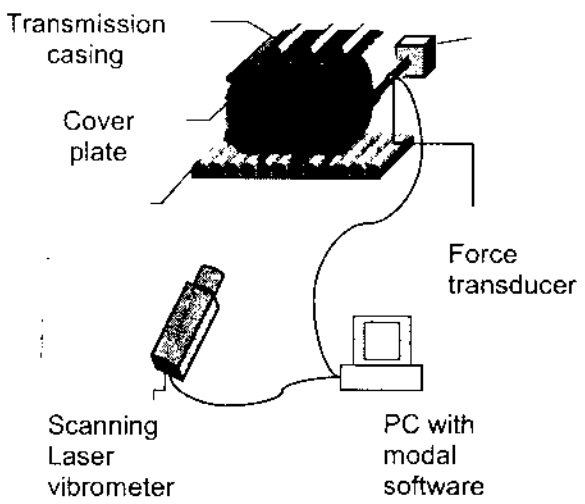

Figure 3. Modal testing of cover plate using shaker excitation and scanning laser vibrometer

SAMPLE RESULTS

Figure 4 shows both a production cover and a modified flat plate. Two versions of the production plate are evaluated: undamped cover and laminated cover. To see the effect of damping treatment, production covers of Figure 4a with and without a damping layer are compared in Figure 5. Most of the peak levels are attenuated by at least 10 dB.

The modified flat plate of Figure 4b is used to understand the effect of partial damping treatment and to develop an analytical model. It also provides convenience in applying damping patches to various locations. Figure 6 illustrates typical effects of the partial damping coverage. As expected, peak levels are attenuated at the first few modes. Downward resonant frequency shifts are also observed. This seems to suggest that the mass loading is dominant.

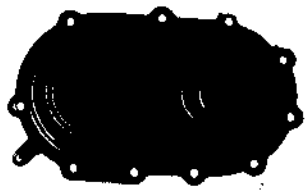

4a) Production cover

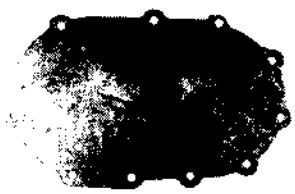

4b) Modified flat plate

Figure 4. Casing cover

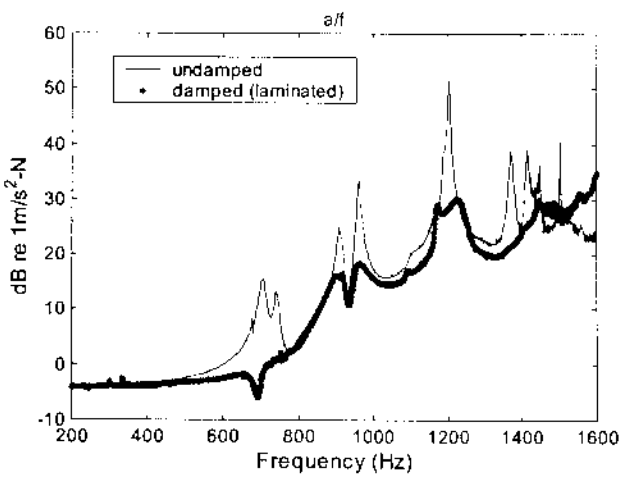

Figure 5. Accelerance spectra of production plates of Figure 4a

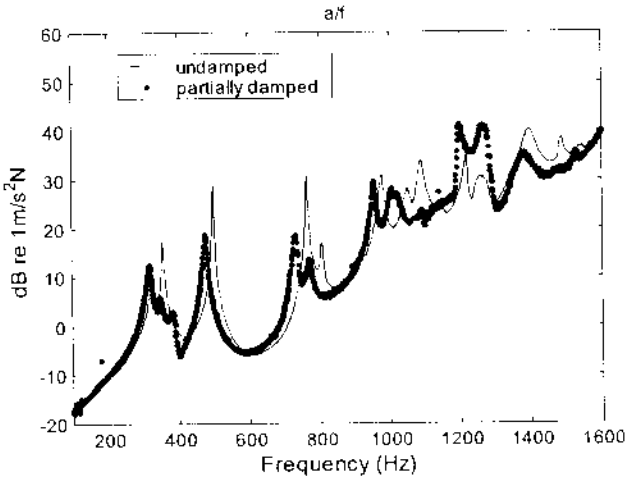

Figure 6. Accelerance spectra of modified flat plate of Figure 4b

EMPIRICAL MODEL

To better understand experimental results, a single degree of freedom empirical model is used. The structural insertion loss (IL_a) may be approximated in terms of changes in loss factor (η) and resonant frequency (f_r). Here, the insertion loss for the r^{th} mode is defined as:

$$IL_a = 20\mathrm{Log}_{10}\left(\frac{a_{undamped}}{a_{damped}}\right)_r \qquad (1)$$

Assume that resonant acceleration (a_r) is given as follows where F_r is the modal force and k_r is the modal stiffness:

$$\left|\frac{a_r}{F_r/k_r}\right| \approx \frac{4\pi^2 f_r^2}{\eta_r} \qquad (2)$$

Hence,

$$IL_a = 20\mathrm{Log}_{10}\left(\frac{\eta_{r,damped}}{\eta_{r,undamped}}\frac{f_{r,undamped}^2}{f_{r,damped}^2}\right) \qquad (3)$$

It is initially assumed that only the mass loading (Δm_r) is introduced by a damping patch, causing a frequency shift (Δf_r). Using the single degree of freedom model, natural frequency f_r of the r^{th} mode of an undamped plate can be calculated by equation (4) where m_r and k_r are the modal mass and stiffness terms.

$$f_r = \frac{1}{2\pi}\sqrt{\frac{k_r}{m_r}} \qquad (4)$$

Addition of mass (Δm_r) only changes equation (4) as follows:

$$1+\frac{\Delta f_r}{f_r} = \sqrt{\frac{1}{1+(\Delta m_r/m_r)}} \qquad (5)$$

Experimental results from different sizes of damping treatments are combined and plotted in Figure 7 using equation (5). Figure 7a summarizes results for mode 1 at around 320 Hz and Figure 7b for mode 2 at around 500 Hz. Observe the limitation of the single degree of freedom empirical model. Equation (5) cannot fully explain measured results, especially the full damping case. The partial damping case data might mean the shift from Equation (5). To correct this result, the actual additional mass needs to be converted to modal mass. This also reveals the fact that the stiffness loading should be considered.

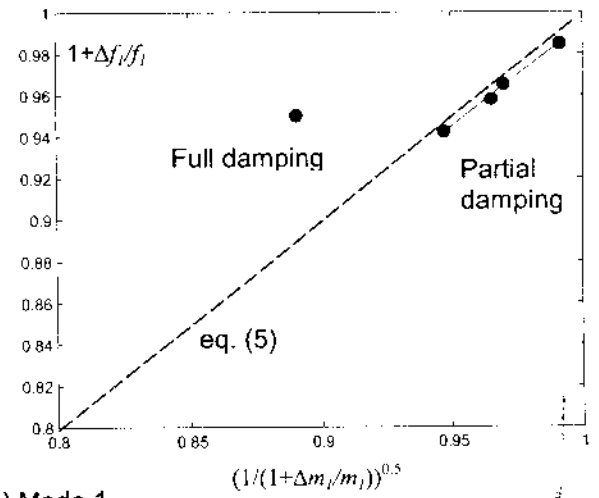

7a) Mode 1

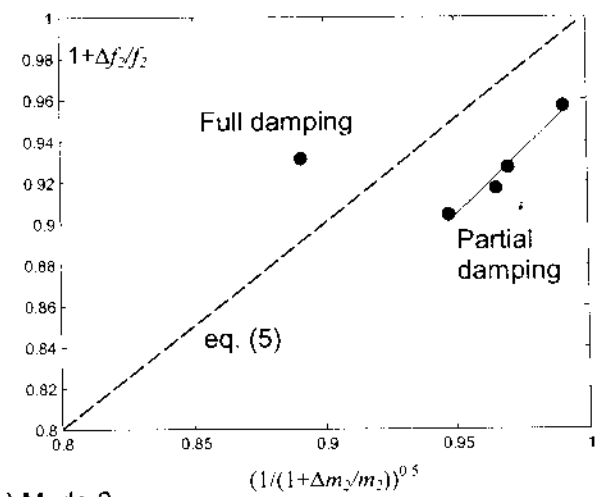

7b) Mode 2

Figure 7. Frequency shift versus patch mass. Key: - - - empirical model, • measured

ANALYTICAL MODEL

For the analytical study, the modified flat plate of Figure 4b is approximated as an elliptical plate with a clamped boundary condition as shown in Figure 8. Modal functions are devised such that they satisfy geometric boundary conditions and are consistent with measured modes [2, 3]. The first five modal functions can be represented as follows. Here, a and b are the dimensions of the elliptical plate, m is the number of nodal lines along major axis (x), n is the number of nodal lines along minor axis (y), A is the modal amplitude bias, and δ is the Kronecker delta function. Each mode is identified by (m,n) indices.

Mode 1 (0,0)

$$\Phi_1(x,y) = (1 - x^2/a^2 - y^2/b^2)^2 \tag{6}$$

Mode 2 (1,0), Mode 4 (0,1), and Mode 5 (1,1)

$$\Phi_{2,4,5}(x,y) = (1 - x^2/a^2 - y^2/b^2)^2 (\delta_{0,m} + \delta_{1,m}\sin(\mathrm{m}\frac{\pi}{a}x))(\delta_{0,n} + \delta_{1,n}\sin(\mathrm{n}\frac{\pi}{b}y)) \tag{7}$$

Mode 3 (2,0)

$$\Phi_3(x,y) = (1 - x^2/a^2 - y^2/b^2)^2 \sin(\frac{\pi}{2a}(3x+a))(x^2/a^2 + A) \tag{8}$$

The symbol A used for mode 3 can be viewed as the modal amplitude bias term since it equalizes each anti-node. Figures 10 and 11 compare experimental and modal function shapes for the first two modes. The possibility of using the modal functions for both undamped and damped cases is ensured by comparing cross-sectional views of undamped and damped mode shapes. One 100 mm circular patch is applied at one anti-node of mode 2 as shown in Figure 9. Shapes of mode 2 are compared in Figure 12 along the major axis (x) of the ellipse (as illustrated in Figure 8).

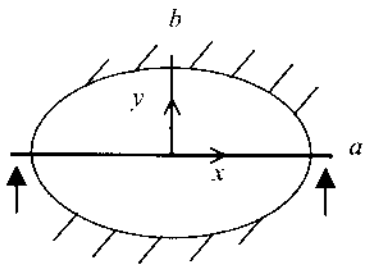

Figure 8. Flat plate idealized as an elliptical plate with clamped boundary

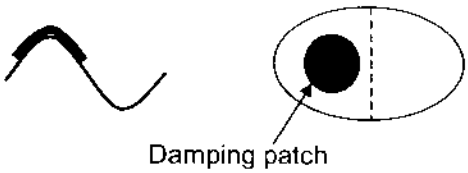

Figure 9. Sample patch location with reference to mode 2

10a)

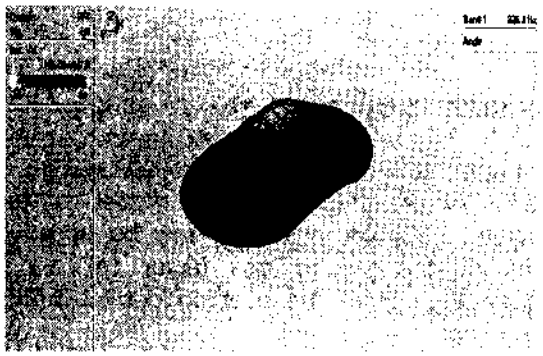

10b)

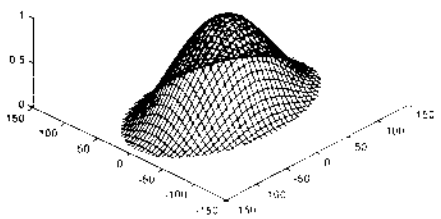

Figure 10. Mode 1 of the flat plate: a) measured, b) assumed modal function

11a)

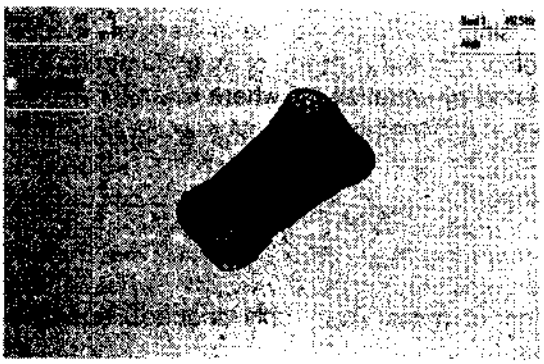

11b)

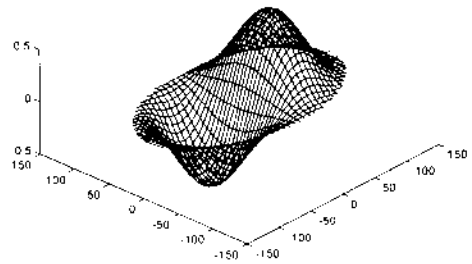

Figure 11. Mode 2 of the flat plate: a) measured, b) assumed modal function

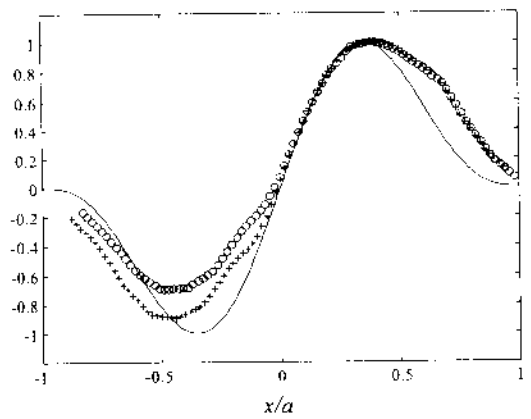

Figure 12. Comparison of shapes for mode 2. Key: -, analytical mode shape; +, measured for an undamped plate; ○, measured for a damped plate

To construct an analytical model, the kinematic relationships between the base plate (#3), damping layer (#2) and constraining layer (#1) is established as shown in Figure 13. Assumptions are as follows [4, 6-8]: (i) the curvature of constraining layer (#1) is the same as the base plate (#3), (ii) the in-plane motion is negligible, (iii) the base plate (#3) and constraining layer (#1) are governed by the Euler's beam equation, (iv) the thickness (h_i) of any layer does not change during deformation. Shear strain of damping layer (#2) can be calculated from the flexural displacement of the base plate (#3). To further simplify the problem, additional assumptions are made: (v) most of the energy dissipation comes from the damping layer (#2), (vi) the energy dissipation of damping layer (#2) is proportional to the strain energy of that layer (U_2), and (vii) the kinetic energy of damping layer (#2) can be neglected. Based on the deformation model and underlying assumptions, strain energy (U_i) of each layer can be described [5] where i=1, 2, and 3.

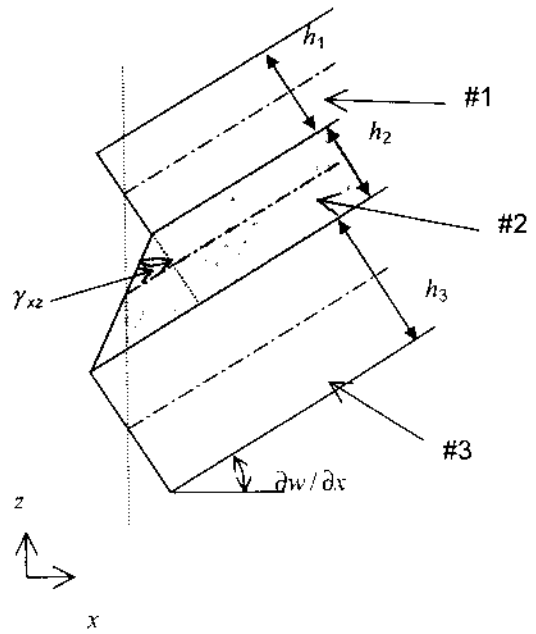

Figure 13. Deformation model of the damped plate where w is the flexural displacement of base plate along z where γ_{xz} is shear strain of damping layer

$$U_i = \left(\frac{E_i h_i^3}{24(1-\nu_i^2)}\right)\int_{i,x}\int_{i,y}\left(\left(\frac{\partial^2 w}{\partial x^2}+\nu_i\frac{\partial^2 w}{\partial y^2}\right)\frac{\partial^2 w}{\partial x^2} + 2(1-\nu_i)\left(\frac{\partial^2 w}{\partial x \partial y}\right)^2 + \left(\frac{\partial^2 w}{\partial y^2}+\nu_i\frac{\partial^2 w}{\partial x^2}\right)\frac{\partial^2 w}{\partial y^2}\right)dydx, \quad i = 1, 3 \tag{9}$$

$$U_2 = U_{2,E} - U_{2,G}, \tag{10}$$

$$U_{2,E} = \frac{E_2 h_2^3}{24(1-\nu_2^2)}\int_{2,x}\int_{2,y}\left(\left(\frac{\partial^2 w}{\partial x^2}+\nu_2\frac{\partial^2 w}{\partial y^2}\right)\frac{\partial^2 w}{\partial x^2} + 2(1-\nu_2)\left(\frac{\partial^2 w}{\partial x \partial y}\right)^2 + \left(\frac{\partial^2 w}{\partial y^2}+\nu_2\frac{\partial^2 w}{\partial x^2}\right)\frac{\partial^2 w}{\partial y^2}\right)dydx$$

$$U_{2,G} = \frac{G_2}{2h_2}\left(\frac{h_1}{2}+\frac{h_3}{2}+h_2\right)^2\int_{2,x}\int_{2,y}\left(\left(\frac{\partial w}{\partial x}\right)^2+\left(\frac{\partial w}{\partial y}\right)^2\right)dydx \tag{11,12}$$

Here, E is the Young's modulus, G is the shear modulus, ν is the Poisson's ratio and w is the flexural deformation along the z axis. Further, $U_{2,E}$ is the strain energy from normal and in-plane shear strains ε_x, ε_y and γ_{xy}, and $U_{2,G}$ is the strain energy from out-of-plane shear strains γ_{xz} and γ_{yz}. Replacing deformation function w with the modal

function (as proposed earlier), one may revise the strain energy ($\overline{U}_i$) based on assumed vibration modes. Next, the kinetic energy (T_i) can be decomposed into translational ($T_{i,T}$) and rotational ($T_{i,R}$) energy.

$$T_i = T_{i,T} + T_{i,R}; \quad i = 1,3 \tag{13}$$

$$T_{i,T} = \frac{1}{2}\rho_i h_i \int_{i,x}\int_{i,y}\left(\frac{\partial w}{\partial t}\right)^2 dydx \tag{14}$$

$$T_{i,R} = \frac{1}{24}\rho_i h_i^3 \int_{i,x}\int_{i,y}\left[\left(\frac{\partial^2 w}{\partial t \partial x}\right)^2 + \left(\frac{\partial^2 w}{\partial t \partial y}\right)^2\right]dydx \tag{15}$$

Here, ρ is the density. If the harmonic motion of a real-valued mode is assumed by the modal function, the maximum kinetic energy at angular frequency ω can be represented as follows. Here, $\overline{T}_i$ can be defined as the kinetic energy expression based on modal displacements.

$$T_{i,\max} = \omega^2 \overline{T}_i; \quad i = 1,3 \tag{16}$$

Further, preliminary calculation shows that $\overline{U}_{2,E}$ and $\overline{T}_{i,R}$ have negligible effects on the overall energy. These terms are therefore dropped for an efficient calculation procedure.

PATCH LOCATION AND SHAPE EFFECTS

Using the analytical model, damping patch location and shape effects are studied for a specific mode. Utilizing assumptions (v) and (vi), the locations where the damping layer of a patch experiences most strain are deemed as optimum patch locations. Figures 14 shows the contour plots of strain energy of the damping layer for mode 1. Here a square patch is used which covers 3.4 % (Γ = 0.034) of the elliptical plate. The damping area ratio (Γ) is defined as the relative area of treatment when applied to one side of the plate without covering the bolts. The plot indicates two optimum points that will cause the damping patch to experience more strain energy than any other location. Mode 1 shape and optimum patch locations from the contour plot are plotted in Figure 15. Figure 16 shows the contour plot for mode 2 where one optimum position at the center of the ellipse may be observed. Figure 17 shows mode 2, its shape and optimum patch location.

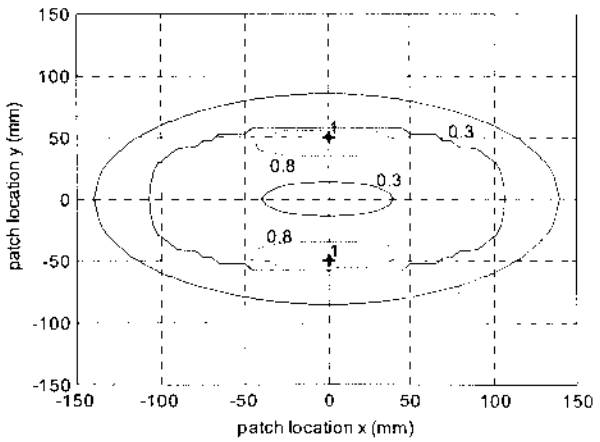

Figure 14. Contour plot of strain energy of damping layer (#2) for mode 1. Numbers are normalized by the value at the optimum point.

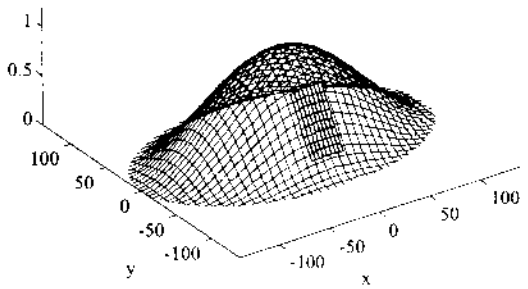

Figure 15. Optimum patch location for mode 1

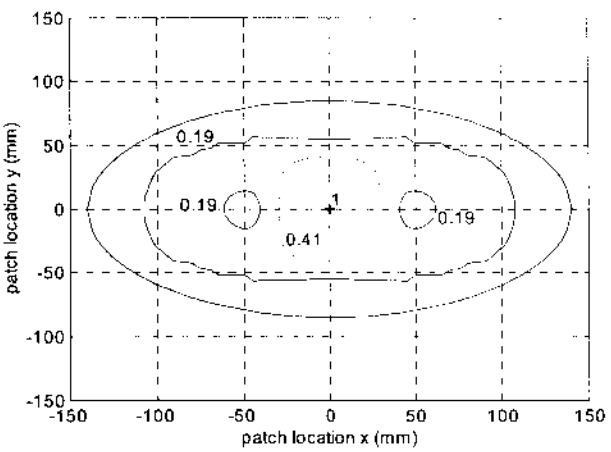

Figure 16. Contour plot of strain energy of damping layer (#2) for mode 2. Numbers are normalized by the value at the optimum point.

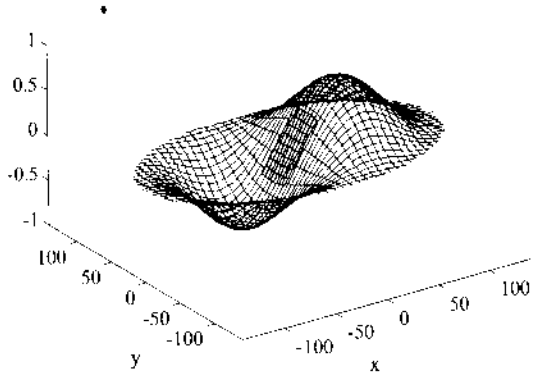

Figure 17. Optimum patch location for mode 2

It can be inferred from these results that the optimum patch location is a point where the slope of modal function is high in order to enhance the shear strain of the damping layer. To attenuate several modes, multiple patches could be applied at or near the optimum points. To understand the shape effect, circular, square and elliptical shapes are compared using the analytical model. All of the patches have the same coverage area. The optimum point does not change. However, there is a slight difference in the strain energy that is experienced by the damping layer at the optimum points. Table 1 compares the relative values at the optimum point for three shapes.

Patch shape	Mode 1	Mode 2
Circular	1.00	1.00
Square	0.99	0.99
Elliptic	1.04	0.96

Table 1. Relative strain energy experienced by the damping layer at the optimum point for three patch shapes of the same area

Elliptic shape seems to be ideal for mode 1 but circular patch can be an optimum shape for mode 2. Such results could be anticipated by observing the shape of the contour plot around the optimum point. For instance, figure 14 shows that the elliptic shape is able to occupy the optimum area more successfully than any other shape. By the same reasoning, better performance of the circular shape over the elliptic one is easily anticipated for mode 2.

Given the material loss factor of damping layer (η_2) and the strain energy of each layer, the loss factor of a damped plate ($\eta_{damped\ plate}$) is computed by following equation since $\eta_1 \approx 0$ and $\eta_3 \approx 0$.

$$\eta_{damped\ plate} = \frac{\sum \eta_i \bar{U}_i}{\sum \bar{U}_i} \approx \frac{\eta_2 \bar{U}_2}{\bar{U}_1 + \bar{U}_2 + \bar{U}_3} \tag{17}$$

The loss factor of the damping layer (η_2) is computed using the following empirical equation that is given by Kung and Singh [6]. Here f is the frequency in Hz.

$$\eta_2 = 2.39\times10^{-1} + 3.54\times10^{-4} f - 7.97\times10^{-7} f^2 + 1.01\times10^{-9} f^3 - 3.32\times10^{-13} f^4 \tag{18}$$

Measured and calculated loss factors are compared in Figure 18. Good agreement is seen over a wide rage of damping area ratio (Γ).

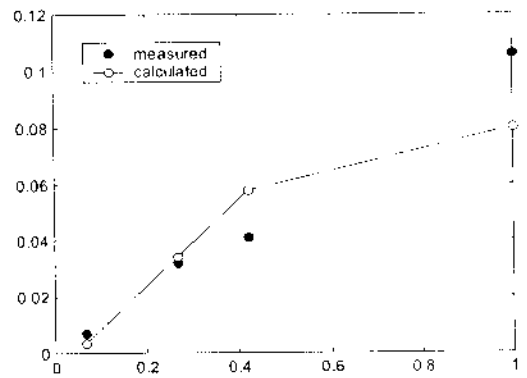

Figure 18. Loss factor ($\eta_{damped\ plate}$) for mode 2. Loss factors are measured by the half-power bandwidth method.

STIFFNESS AND MASS LOADING EFFECTS

Downward shifts in natural frequencies ($-\Delta f$) introduced by the applied damping patch are examined next. Two damping patches are attached at the anti-nodes of mode 2 and their areas are varied. Measured data is compared with calculations assuming the following relation. If a natural frequency (f_r) without any damping treatment is defined by equation (19), its frequency shift (Δf_r) can be related to the ratio of strain to kinetic energies like equation (20). This ignores the strain energy contribution from the damping layer (#2) because it is compliant. For the r^{th} mode:

$$(2\pi f_r)^2 = \left(\frac{\bar{U}_3}{\bar{T}_3}\right)_r \tag{19}$$

$$(2\pi(f_r + \Delta f_r))^2 = \left(\frac{\bar{U}_3 + \bar{U}_1}{\bar{T}_3 + \bar{T}_1}\right)_r \tag{20}$$

$$\frac{\Delta f_r}{f_r} = \left(\frac{1 + (\bar{U}_1/\bar{U}_3)_r}{1 + (\bar{T}_1/\bar{T}_3)_r}\right)^{0.5} - 1 \tag{21}$$

Observe that $\bar{U}_1/\bar{U}_3$ is an indication of the stiffness loading and $\bar{T}_1/\bar{T}_3$ quantifies the mass loading. From equation (21), frequency shift can be controlled by

changing the mechanical properties of the constraining layer (#3). Figure 19 compares the measured and calculated frequency shifts ($-\Delta f$). This plot illustrates an improved prediction over the single degree of freedom empirical model that only considers the mass loading effect.

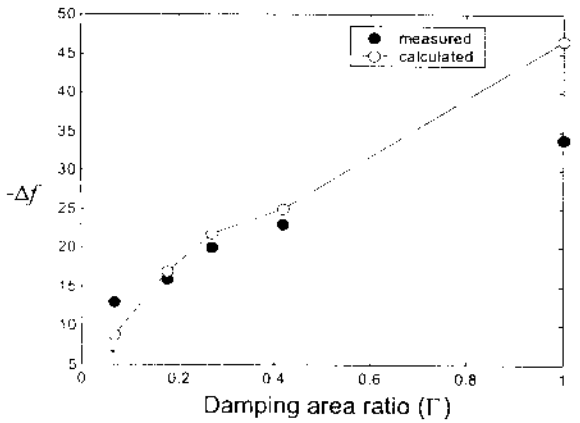

Figure 19. Measured and calculated frequency shifts ($-\Delta f$, Hz) for mode 2

CONCLUSION

To achieve optimum performance, a patch should be located such that it produces most shear strain in the damping layer from the analytical study. Patch shape can be decided by examining the contour plot of strain energy and optimum points. Frequency shifts can be predicted by examining the ratio of kinetic and potential energies that quantify mass and stiffness loading effects, respectively. This simplified analytical model is based on the assumed modal functions that assume exact in-phase or out-of-phase vibratory motions. As a result, complex mode shapes cannot be precisely predicted. Depending on the rigidity of a constraining layer, the validity of assumption (i) needs to be re-examined. In particular, the transfer of bending moment from the base plate to the constraining layer may not be effective due to the compliance of the in between damping layer. To examine this, a simple finite element model is examined for a clamped-free beam with a damping patch. Damping layer is incorporated as a thin compliant layer compared with the constraining layer. Stiffness of constraining layer is assumed to be same as the beam. Figure 20 shows the location of the damping patch with respect to the second vibration mode of beam.

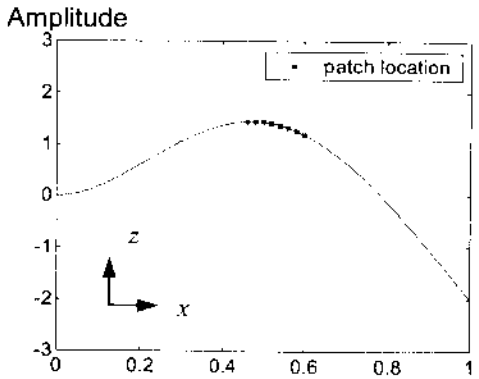

Figure 20. Patch location given the second vibration mode of a clamped-free beam based on finite element model

Figure 21 illustrates normal stress (σ_z) as well as shear stress (τ_{xz}) in the damping layer, which shows the important role of normal strain in partially covering constrained layer damping treatment. Insufficient deformation of constraining layer is believed to be the reason why normal stresses are seen.

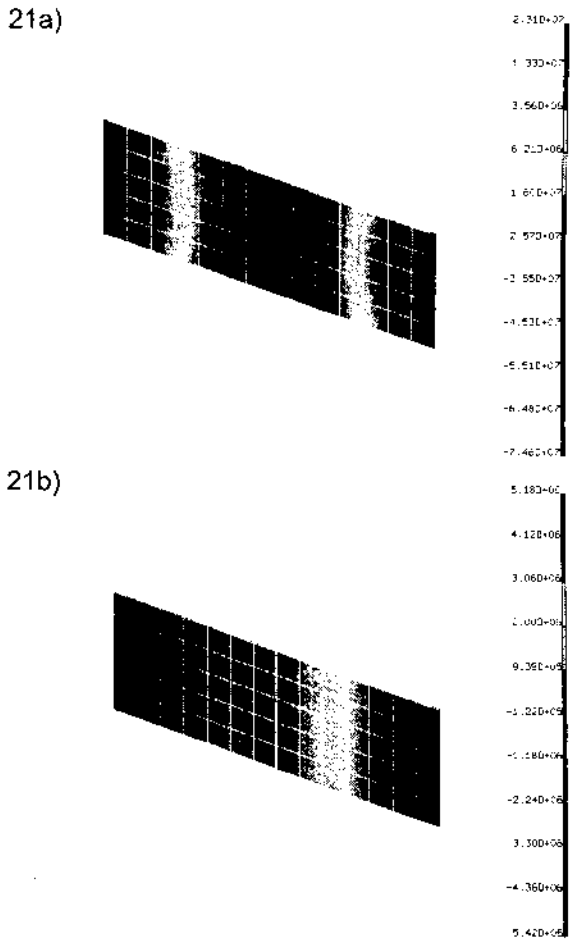

Figure 21. Stresses within the damping layer based on a finite element model a) σ_z and b) τ_{xz}

Future work should include material properties of the damping layer. Frequency-varying loss factors of extensional and shear deformations would need to be provided. More realistic deformation models of the damping patches should be developed.

ACKNOWLEDGMENTS

The authors gratefully acknowledge the financial support from the Center for Automotive Research (CAR) and its industrial consortium in noise, vibration and dynamics thrust (Bosch, Delphi, Dow, EWI, Fiat CRF, Ford, General Motors and LuK).

REFERENCES

1. D. Crimaldi, "Vibro-acoustic studies of irregular plates with complex boundaries", M.S. Thesis, The Ohio State University, 1997
2. A. Leissa, "Vibration of plates," Acoustical Society of America, 1993
3. R. D. Blevins, "Formulas for natural frequency and mode shape", Van Nostrand Reinhold Company, 1979
4. E. M. Kerwin, Jr. "Damping of flexural waves by a constrained viscoelastic layer," *Journal of the Acoustical Society of America* **31**, 952-962, 1959.
5. A. C. Ugural, S. K. Fenster, "Advanced strength and applied elasticity", Prentice Hall PTR, 1995
6. S. W. Kung and R. Singh, "Vibration analysis of beams with multiple constrained layer damping patches," *Journal of Sound and Vibration* **212**(5), 781-805, 1998
7. S. W. Kung and R. Singh, "Complex eigensolutions of rectangular plates with damping patches," *Journal of Sound and Vibration* **216**(1), 1-28, 1998
8. S. W. Kung and R. Singh, "Development of approximate methods for the analysis of patch damping design concepts," *Journal of Sound and Vibration* **219**(5), 785-812, 1999

CONTACT

Web address:
http://rclsgi.eng.ohio-state.edu/~singh/ADL.html

LIST OF SYMBOLS

Symbols

A	modal amplitude bias
a	acceleration
a	major axis dimension
b	minor axis dimension
f	frequency (Hz)
Δf	frequency shift (Hz)
E	Young's modulus
F	input force
G	Shear modulus
h	thickness
k	stiffness
m	mass
Δm	mass loading
m	number of nodal lines along x
n	number of nodal lines along y
T	kinetic energy
$\overline{T}$	kinetic energy expression based on modal displacement
U	strain energy
$\overline{U}$	strain energy expression based on modal function
w	flexural deformation
ε	extensional strain
Φ	modal function
γ	shear strain
Γ	damping area ratio
η	loss factor
ν	Poisson's ratio
ρ	density
ω	frequency (rad/s)
IL_a	insertion loss

Subscripts

1, 2	mode 1 or 2
i	layer index
r	modal index
R	rotational
T	translational